RSC Advances

PAPER

View Article Online
View Journal | View Issue

Cite this: *RSC Adv.*, 2021, **11**, 6699

An electrochemical immunosensor coupling a bamboo-like carbon nanostructure substrate with toluidine blue-functionalized Cu(II)-MOFs as signal probes for a C-reactive protein assay

Mei Li, Xiaojuan Xia, Shuang Meng, YuChan Ma, Tong Yang, Yunhui Yang* and Rong Hu*

Received 8th November 2020
Accepted 18th January 2021

DOI: 10.1039/d0ra09496j

rsc.li/rsc-advances

In this paper, a novel sandwich immunosensor based on a toluidine blue (Tb) loaded metal organic framework (Cu(II)-HKUST-1/Tb) as the signal element and a nitrogen-doped 3D carbon nanostructure as the electrode substrate was constructed for the detection of C-reactive protein (CRP). Tb as an electrochemically active agent usually forms a polymer by aggregation in the solvent, causing a poor electrochemical response. Therefore, in order to overcome this obstacle, Cu(II)-HKUST-1 with a porous nanostructure and large specific surface area as a carrier could adsorb a large number of Tb molecules on its surface to improve its electrochemical performance. In addition, the high electron transfer efficiency of the N-doped bamboo-like carbon nanotubes (CoFe/N-GCT) improves the sensitivity of the biosensor. Differential pulse voltammetry (DPV) was used to detect the current signal of Tb at −0.2 V. The current response increased with the increase in concentration of CRP, ranging from 0.5 to 200 ng mL^{-1}. The detection limit is 166.7 pg mL^{-1} (S/N = 3). Moreover, the proposed biosensor can be applied in real serum sample detection. It has potential applications in the field of biomedicine assays.

Introduction

C-reactive protein (CRP) is produced by hepatocytes under the regulation of cytokines such as interleukin-6,[1] tumor necrosis factor, interferon and so on. It is a member of the pentapeptide protein family.[2] Its concentration rises rapidly in the acute phase during inflammation. Some acute and chronic infections, *e.g.* organ transplantation, bacterial or viral infections, malignant tumors, tissue damage, atherosclerosis and other body injuries can cause a sharp rise in CRP.[3,4] Serum CRP is not only a predictor of cardiovascular disease, but is also a powerful monitoring index of coronary heart disease and other diseases.[5] Recently, coronavirus disease (COVID-19) has become a global focus, the numbers of infections and deaths from the virus are still rising, and asymptomatic infected people have become a potential source of infection in the population. Studies show that there is a positive correlation in coronavirus disease patients between CRP levels in the early stages of the disease and lung lesions[6] so we have to admit that the clinical monitoring of serum CRP levels is necessary for preventing diseases. As the concentration of serum CRP causing inflammation and disease infection is very low,[7] it is particularly important to develop an ultrasensitive method for the detection of CRP.

For the clinical detection of CRP, researchers have developed many technologies such as the turbidimetric method,[8,9] fluorescence method,[10] colorimetric method,[11] radiation and enzyme-linked immunosorbent assay.[12] Although these methods show a good performance, most of them require high cost instruments. Electrochemical immunosensors have been widely applied in various fields because of their high sensitivity, low cost, simplicity and convenience.

In order to construct an immunosensor with a good analytical performance, the modified material on the electrode surface requires high conductivity, high specific surface area and good bioconjugation abilities. Since the discovery of carbon nanotubes (CNTs) in 1991,[13] they have been widely used in many fields, such as biomedicine,[14] optical bioimaging,[15] new energy batteries,[16] biosensors and so on, due to their good mechanical stability, high electrical conductivity,[17,18] and excellent optical and thermal properties. Based on the unique advantages of carbon nanotubes, CoFe alloy nanoparticles embedded in N-doped carbon nanotubes combined with flexible rGO to form a three-dimensional (3D) nanomaterial (CoFe/N-GCT) were synthesized as a substrate. Previously reported studies have shown[16] that doping N in the carbon nanotube system can significantly improve the electron transfer efficiency of the carbon nanotubes. Reduced graphene oxide (rGO)[19]

College of Chemistry and Chemical Engineering, Yunnan Normal University, Kunming, 650500, China. E-mail: yyhui2002@aliyun.com; hudierong_168@163.com; Fax: +86 871 65941086

together with carbon nanotubes as the carbon source of the conductive network can further improve the electric conductivity. Gold nanoparticles (Au NPs) bound to the surface of CoFe/N-GCT can immobilize biological macromolecules. Based on this excellent performance, Au NPs loaded on the 3D composite CoFe/N-GCT can be used to immobilize the CRP antibody and enhance the electrical conductivity of the nanocomposite.

For sandwich immunosensors, the stability of the electroactive substance is also an important factor affecting the performance of the sensors. Toluidine blue (Tb) is a kind of electroactive substance,[20] which can be used as a signal source of the immunosensors. As an electroactive material, Tb has a high signal output, a low false negative rate, a low price, and so on. However, Tb tends to aggregate in the solvent to form a polymer.[21] The existence of the polymer reduces the electron transfer ability of the electroactive biomolecules and the production and lifetime of active oxygen (especially singlet oxygen) weakens its analytical performance, shortens its service life, and limits the development of the clinical applications of Tb. Therefore, it is necessary to improve the stability of Tb. As a new type of porous material, metal organic frameworks (MOFs) with functionalized pore surfaces,[22,23] good structural adjustability and high specific surface areas have attracted great attention in many fields[24–27] such as biosensors. In this paper, Cu(II)-HKUST-1 formed by Cu^{2+} and trimesic acid (H_3BTC) is selected as the signal tag carrier due to its large specific surface area, large pore volume, strong structural adaptability, good hydrothermal stability and uniform pore size distribution.[28–30] It can load a large number of Tb molecules in the channel of the MOFs, reducing the degree of polymerization of Tb. Au NPs were modified on Cu(II)-HKUST-1 to enhance the stability of these MOFs. Therefore, the high stability of Au NPs/Cu(II)-HKUST-1 loaded with many Tb molecules can amplify the electrochemical signal, improving the sensitivity of the biosensors.

In this work, a novel sandwich immunosensor based on Au NPs/Cu(II)-HKUST-1/Tb and CoFe/N-GCT was constructed for the detection of CRP (Scheme 1). Au NPs/CoFe/N-GCT was used as the substrate. The 3D nanostructure with a high surface area can load generous amounts of anti-CRP *via* Au–S bonds. A composite material (Au NPs/Cu(II)-HKUST-1/Tb) formed by a copper MOF with Tb was used as a biomarker which has a stable and strong electrochemical signal. In the presence of CRP, the electrochemical signal of Tb is detected by using differential pulse voltammetry (DPV) to realize the quantitative determination of target. The current response is increased with the increase in the concentration of CRP, ranging from 0.5 ng mL^{-1} to 200 ng mL^{-1}. The biosensor has high selectivity, sensitivity, stability, reproducibility and regeneration performance with repeated use. The detection limit of 166.7 pg mL^{-1} (S/N = 3) was obtained. Moreover, the proposed biosensor could be applied in real serum sample detection. This biosensor could become an attractive platform in bioanalysis of proteins and other molecules.

Experimental section

Reagents and apparatus

C-reactive protein antigen (CRP) and C-reactive protein antibody (anti CRP) were purchased from Shanghai Linc-Bio Co., Ltd (Shanghai, China); toluidine blue (Tb), melamine

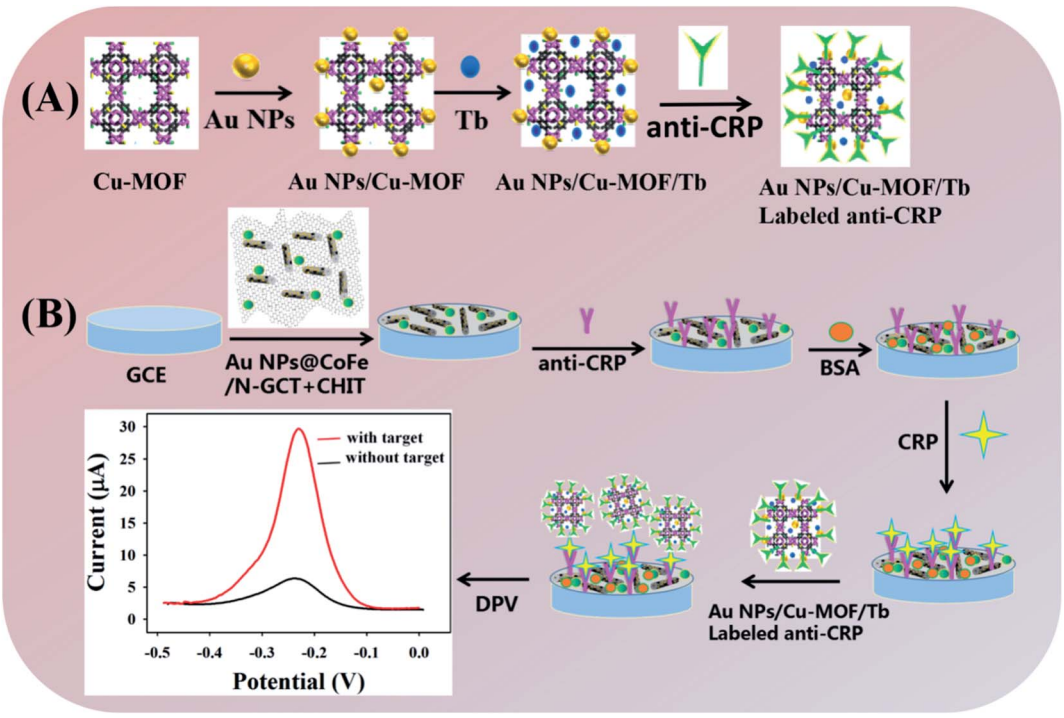

Scheme 1 An illustration of a CRP sandwich immunosensor. (A) The fabrication of CRP antibody-labelled Au NPs/Cu(II)-HKUST-1/Tb. (B) The analytical procedure toward CRP using a CRP sandwich immunosensor in this work.

($C_3H_6N_6$), cobalt chloride hexahydrate ($CoCl_2 \cdot 6H_2O$), graphene oxide (GO), and copper acetate ($Cu(CH_3COO)_2 \cdot H_2O$) were purchased from Shanghai Yuanye Biological Co., Ltd (Shanghai, China); trimesic acid ($C_9H_6O_6$) was purchased from Aladdin Industrial Corporation Co., Ltd (Shanghai, China); bovine serum albumin (BSA), 1-ethyl-(3-dimethylaminopropyl) carbodiimide hydrochloride (EDC), and thioacetamide (C_2H_5NS) *N*-hydroxysuccinimide (NHS) were purchased from Sigma-Aldrich (Missouri, USA); $HAuCl_4 \cdot xH_2O$ was obtained from J&K Scientific Co., Ltd (Beijing, China). The reagents used in this experiment were analytical grade, and the water used was ultrapure water.

Apparatus

Differential pulse voltammetry (DPV), cyclic voltammetry (CV) and electrochemical impedance spectroscopy (EIS) were measured by a CHI 660D-electrochemical workstation (Chenhua Instruments Co., Ltd., Shanghai, China). Transmission electron microscopy imaging (TEM) was obtained by a JEM-2100 transmission electron microscope (JEOL Co., Ltd., Japan), Scanning electron microscopy (SEM) and element energy spectrum analysis were carried out by a quanta-200 scanning electron microscope (Hitachi Science Systems Co., Ltd Japan). X-ray photoelectron spectroscopy (Thermo Fisher Scientific Co., Ltd., Shanghai, China) was used to obtain the XRD patterns. The electrochemical detection in the experiment was carried out using a three-electrode system, in which the glassy carbon electrode was the working electrode, the saturated calomel electrode was the reference electrode, and the platinum electrode was the counter electrode.

Synthesis of the CoFe/N-GCT nanocomposites

At room temperature, 24 mmol melamine was dispersed in 25 mL deionized (DI) water using expanded graphite as the raw material to obtain a melamine solution. Subsequently, the solution was mixed with 10 mL of 0.2 mol L^{-1} $K_3[Fe(CN)_6]$ aqueous solution and stirred for 1 h. 15 mL of an aqueous solution containing 3 mmol of cobalt chloride was added dropwise to the above solution while stirring and then stirred for another half an hour to obtain a Prussian Blue Analogue (PBA)-melamine precursor. 40 mg of graphene (GO) was dispersed in 30 mL of DI water, ultrasonically treated to obtain a brown solution, mixed with the above solution, stirred for 2 h, centrifugally filtered, and dried at 60 °C to obtain a solid powder of the Prussian Blue Analogue (PBA)-melamine-GO precursor. Next, PBA-melamine-GO was carbonized at 350 °C for 1 h and then treated at a heating rate of 5 °C per minute for 2 h in an N_2 environment (900 °C) to synthesize CoFe/N-GCT.[31]

Synthesis of the gold nanoparticles

50 mL of DI water and 500 μL of 1% $HAuCl_4$ were added into a round bottom flask. When the mixture was uniformly dispersed under ultrasound and heated and stirred until boiling, 1% trisodium citrate (1.75 mL) was quickly added to the flask, which was heated for 20 min. When the solution turned a wine-red colour, heating was stopped. Then, the mixture was cooled down to room temperature and stored at 40 °C for standby.[32]

Synthesis of the Au NPs/CoFe/N-GCT nanocomposites

50 mg of the CoFe/N-GCT solid was weighed and put into a 250 mL three-necked flask. Then, 10 mL of DI water was added and uniformly dispersed ultrasonically. Next, 20 mL of the Au nanosol was added dropwise into the flask with a Soxhlet extractor followed by stirring at normal temperature for 24 h to fully absorb the Au NPs. After centrifuging, washing with DI water three times and vacuum drying, the Au NPs/CoFe/N-GCT nano composite material was obtained.

Synthesis of Cu(II)-HKUST-1

First, 0.4200 g of trimesic acid was added to a 250 mL three-necked flask. Then, 40 mL of absolute ethyl alcohol was added to dissolve the pyromellitic acid to obtain solution A. Subsequently, 0.6000 g of copper acetate was weighed in a 100 mL beaker, and 40 mL of DI water and 4 mL of glacial acetic acid were simultaneously added to dissolve to obtain solution B. Under stirring at room temperature, a Soxhlet extractor was used to add solution B dropwise to solution A. After dropwise addition and continuous stirring for 1 h at room temperature, centrifugation was carried out followed by washing with water and ethanol three times, respectively. Finally, Cu(II)-HKUST-1 nanoparticles were obtained after being centrifuged and vacuum dried at 40 °C for 48 h.[33]

Synthesis of Au NPs/Cu(II)-HKUST-1

50 mg of the Cu(II)-HKUST-1 solid powder and 10 mL of DI water were added into a 250 mL three-neck flask followed by uniformly dispersing with ultrasound. Then, 20 mL of the Au nanosol was added dropwise into the flask using a Soxhlet extractor and stirring at normal temperature for 24 h to fully absorb the Au nanoparticles. After centrifugation, washing with DI water three times, and vacuum drying, the Au NPs/Cu(II)-HKUST-1 nanocomposite material was obtained.

Labeling the CRP antibody with Au NPs/Cu(II)-HKUST-1/Tb

17 mg of Au NPs/Cu(II)-HKUST-1 and 1 mg of Tb were dispersed in 1 mL DI water. After stirring at room temperature for 12 h, centrifugation and washing with DI water twice, it was dispersed in 1 mL of PBS. Then, 200 μL of 50 mmol L^{-1} NHS, 200 μL of 50 mmol L^{-1} EDC and 10 μL of 1 mg mL^{-1} CRP antibody were respectively added to the above solution, placed in a shaker at 4 °C and shaken for 12 h. Then, 25 μL of 10% BSA was added. After being shaken for 30 min, centrifuged, and washed twice with PBS containing 25 mmol L^{-1} NaCl, the above precipitate was dispersed in 1 mL of 0.01 mol L^{-1} PBS (pH 7.4) and stored at 4 °C for later use.

Preparation of the C-reactive protein immunosensor

A glassy carbon electrode (GCE, $\varphi = 3$ mm) was polished using Al_2O_3 powder with particle sizes of 1.5 nm, 0.5 nm and 50 nm in turn. Then, GCE was ultrasonically washed in a nitric acid

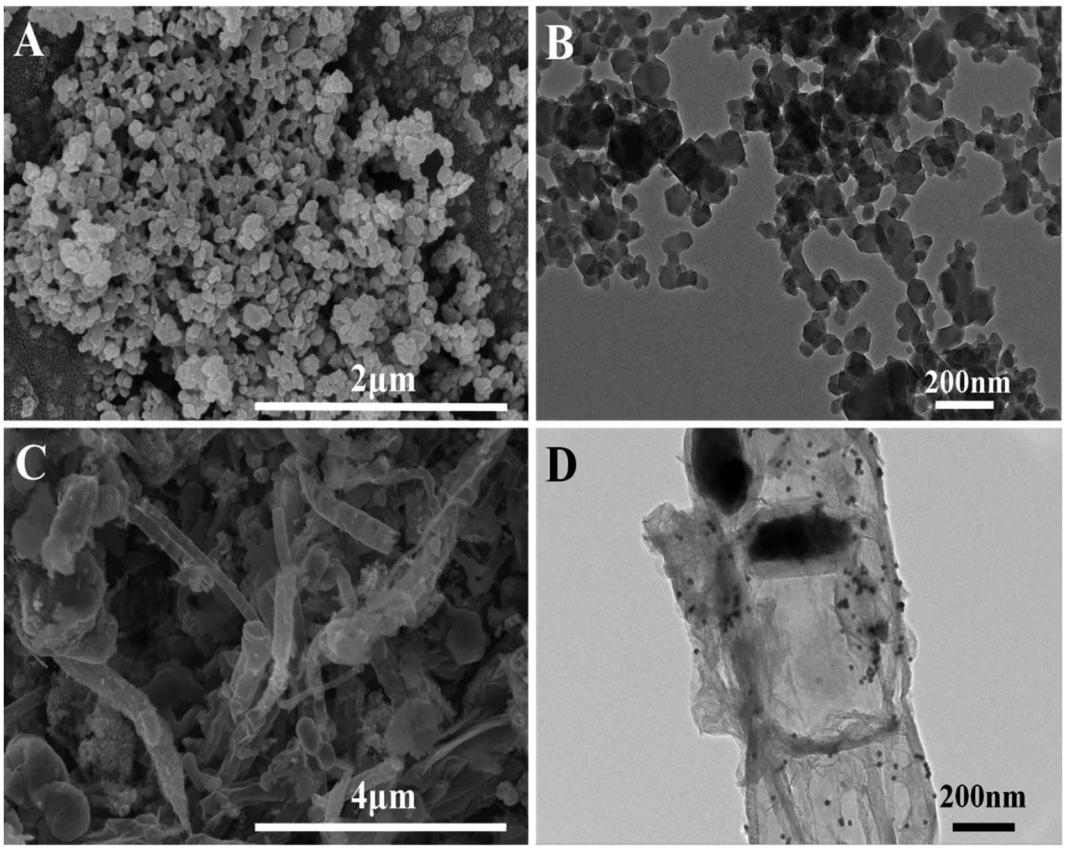

Fig. 1 SEM (A) and TEM (B) images of Cu(II)-HKUST-1; SEM (C) and TEM (D) images of Au NPs/CoFe/N-GCT.

aqueous solution (V (HNO_3) : V (H_2O) = 1 : 1), anhydrous ethanol and DI water for 5 min, respectively, and dried in the air. Subsequently, 0.5% chitosan and 5 mg mL^{-1} Au NPs@CoFe/N-GCT were mixed evenly with the ratio of 1 : 5. Then 10 μL of the above mixed liquid was added to the surface of the treated bare electrode and air dried. Next, 10 μL of the 40 μg mL^{-1} CRP antibody was added to the surface of the electrode, placed in a refrigerator and left overnight at 4 °C. After the anti-CRP/AuNPs@CoFe/N-GCT/CHIT modified GCE was washed with PBS buffer solution for three times, 10 μL of 1% BSA solution was added dropwise on the electrode in a 37 °C incubator for 1 h to block the non-specific binding site. Next, the electrode was washed three times with PBS solution and dried in air. Then, CRP antigens with different concentrations were dropped on the immunosensor, placed in an incubator at 37 °C for 1 hour, then washed with PBS for three times. After air drying, 10 μL of the CRP antibody labeled with the Au NPs/Cu(II)-HKUST-1/Tb nanomaterial was dropped on the electrode, placed in an incubator at 37 °C for 45 min, washed with PBS for three times and dried. The CRP immunosensor (labeled anti-CRP/CRP/BSA/anti-CRP/Au NPs@CoFe/N-GCT/GCE) was obtained. The preparation schematic diagram of the CRP immunosensor is shown in Scheme 1.

Detection method

The prepared immunosensor was put into a small beaker filled with 10 mL PBS buffer solution. Using the immunosensor as a working electrode, DPV was carried out within the voltage range of −0.5 to 0.1 V with 50 mV amplitude, 0.05 s pulse time and 0.2 s pulse period to realize the quantitative determination of CRP.

Results and discussion

Micromorphology characterization of Cu(II)-HKUST-1 and Au NPs/CoFe/N-GCT nanocomposites

Fig. 1(A) shows the SEM morphology of Cu(II)-HKUST-1, from which it can be observed that Cu(II)-HKUST-1 nanoparticles are intertwined to form a grid structure with voids with different pore sizes. Fig. 1(B) is a TEM morphological characterization diagram of Cu(II)-HKUST-1, from which it can be seen more clearly that Cu(II)-HKUST-1 nanoparticles are relatively uniform and present the shape of nanosheets. The Au NPs/CoFe/N-GCT composite nanomaterials were characterized by SEM, as shown in Fig. 1(C), in which the tubular Au NPs/CoFe/N-GCT composite nanomaterials can be clearly observed. In addition, the micromorphology of the Au NPs/CoFe/N-GCT composite nanomaterials was characterized by TEM. It can be seen from Fig. 1(D) that the CoFe alloy is embedded on the N-GCT, and the CoFe/N-GCT composite adsorbs gold nanoparticles so that they are uniformly loaded on the surface.

Characterization of the Cu(II)-HKUST-1 nanoparticles by X-ray diffraction (XRD)

In this experiment, the structure of the Cu(II)-HKUST-1 nanoparticles was characterized by XRD. The result is shown in

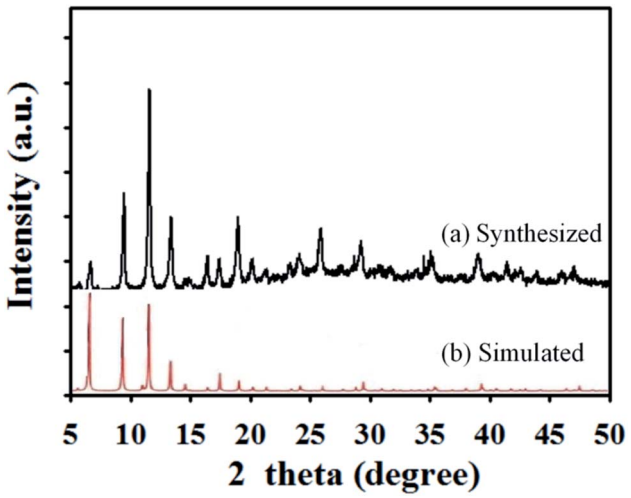

Fig. 2 X-ray diffraction of Cu(II)-HKUST-1 (a: synthesized; b: simulated).

Fig. 2. The characterization results are consistent with the results of Cu(II)-HKUST-1 reported in the literature,[33] indicating that the Cu(II)-HKUST-1 nanoparticles have been successfully synthesized in this experiment.

Energy spectrum analysis of the CoFe/N-GCT nanocomposites

In addition to TEM and SEM characterization, the CoFe/N-GCT nanocomposites synthesized in this experiment were also characterized by elemental energy spectrum analysis (EDS). Fig. 3 confirms that the carbon nanotubes synthesized in this experiment are embedded with the CoFe alloy, which is consistent with the TEM characterization results. In addition, the CoFe alloy coexists with nitrogen, carbon and oxygen elements introduced during the synthesis of this material, and their element contents are shown in table, which once again confirms that CoFe/N-GCT was successfully synthesized in this experiment.

Experimental feasibility analysis

In order to explore the rationality of the experimental scheme, the feasibility analysis is made in the preliminary stage of the experiment. Fig. 4 shows the DPV response curves of the sandwich immunosensor in PBS buffer solution with and without CRP.

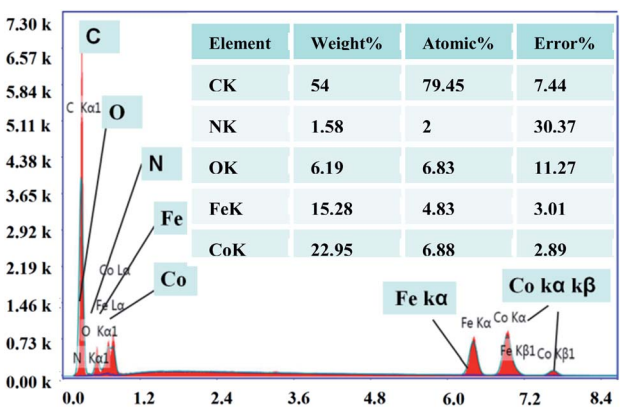

Element	Weight%	Atomic%	Error%
CK	54	79.45	7.44
NK	1.58	2	30.37
OK	6.19	6.83	11.27
FeK	15.28	4.83	3.01
CoK	22.95	6.88	2.89

Fig. 3 Energy spectrum analysis diagram of the CoFe/N-GCT nanocomposites. The inset table: contents of elements in the CoFe/N-GCT nanocomposites.

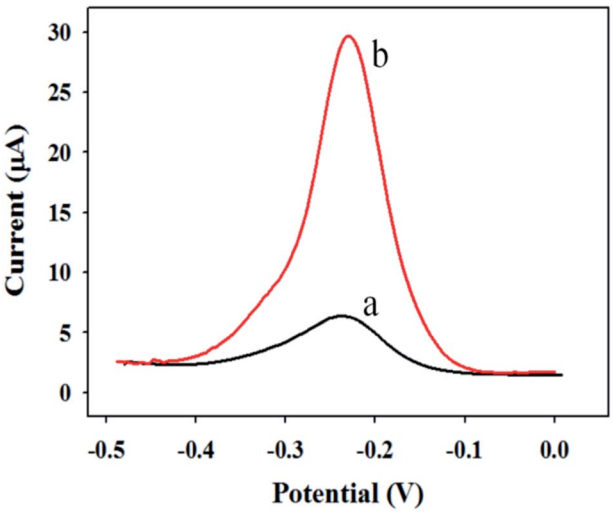

Fig. 4 DPV response curves of the sandwich immunosensor in PBS buffer solution (a: without CRP; b: with 200 ng mL^{-1} of CRP).

Curve *a* is the DPV response curve without detection of the target CRP antigen. Curve *b* is the DPV response curve when adding 200 ng mL^{-1} to detect the target CRP antigen. As can be seen from the figure, when the detection target is added, the current response signal obviously increases relative to the blank, which proves that the experimental design scheme is feasible.

Electrical conductivity analysis of Au NPs/CoFe/N-GCT

Au NPs/CoFe/N-GCT was synthesized *via* CoFe alloy nanoparticles tangled with reduced graphene oxide (rGO) nanosheets. In order to explore the electrical conductivity of the composite carbon nanotubes, the conductivity of CNTs, rGO and Au NPs/CoFe/N-GCT was tested by AC impedance behavior, and the AC impedance spectra of the test results of the three

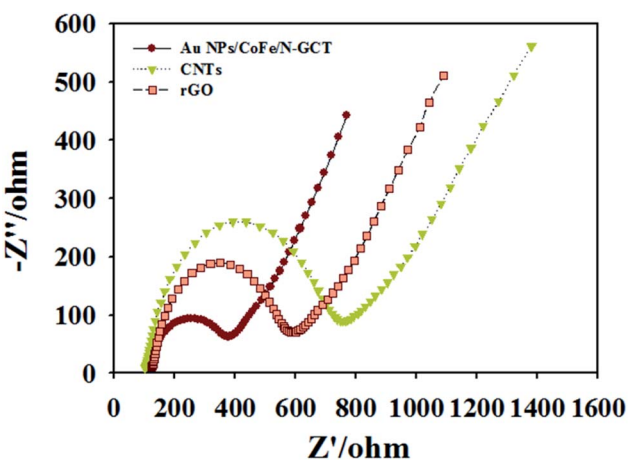

Fig. 5 AC impedance spectra of Au NPs/CoFe/N-GCT, rGO and CNTs.

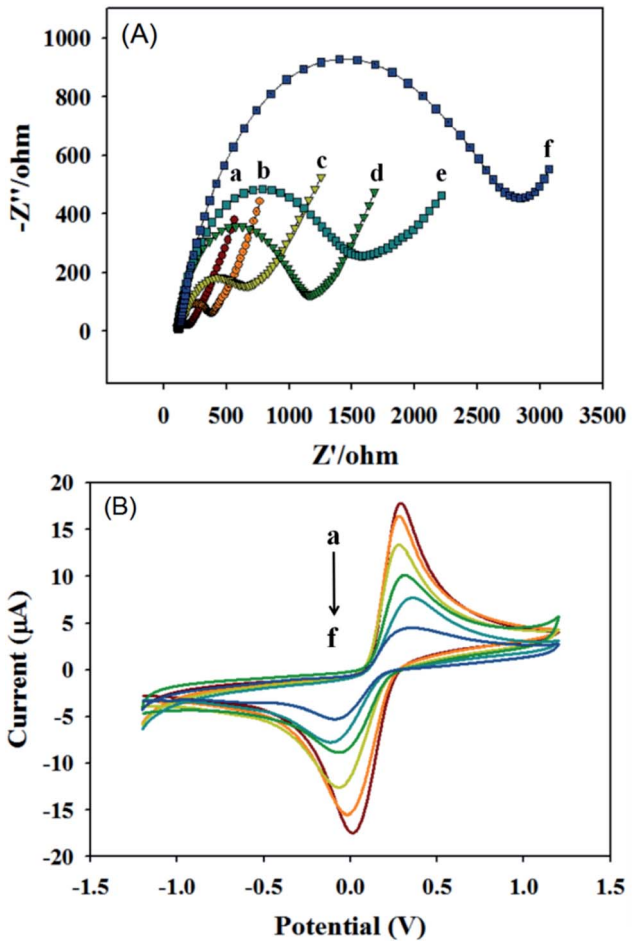

Fig. 6 (A) AC impedance and (B) cyclic voltammetric curves measured at 5 mmol L^{-1} $[K_3Fe(CN)_6]/K_4Fe(CN)_6$ with different modified electrodes (a): bare GCE; (b): Au NPs@CoFe/N-GCT/CHIT/GCE; (c) anti-CRP/Au NPs@CoFe/N-GCT/CHIT/GCE; (d): BSA/anti-CRP/Au NPs@CoFe/N-GCT/CHIT/GCE; (e) CRP/BSA/anti-CRP/Au NPs@CoFe/N-GCT/CHIT/GCE; and (f) labeled anti-CRP/CRP/BSA/anti-CRP/Au NPs@CoFe/N-GCT/CHIT/GCE.

materials are shown in Fig. 5. The impedance values of CNTs (700 Ω) and rGO (500 Ω) are both larger than that of Au NPs/CoFe/N-GCT (300 Ω), indicating that Au NPs/CoFe/N-GCT has better conductivity and electron transfer efficiency. Therefore, Au NPs/CoFe/N-GCT was chosen as the electrode substrate.

AC impedance behavior and cyclic voltammetry behavior of different modified electrode surfaces

In the layer-by-layer modification process of the sensor is the key to successfully constructing the sensor so electrochemical impedance spectroscopy (EIS) and cyclic voltammetry were used to characterize the electrode interfaces with different modifications. Fig. 6(A) is the impedance curves of different electrode modified interfaces measured in 5 mmol L^{-1} of $K_3Fe(CN)_6/K_4Fe(CN)_6$ solution. Among them, curve a is the AC impedance curve of bare GCE, which is almost a straight line because its resistance is small and its conductivity is extremely strong, demonstrating that diffusion controlled the electron transfer. Curve *b* is the AC impedance curve of GCE modified with the Au NPs@CoFe/N-GCT/CHIT composite material. The electrochemical impedance increased (R_{ct} = 480 Ω) compared with that of curve a because chitosan is contained in the material covered by the electrode surface, which hinders the transfer of electrons on the electrode surface and weakens the conductivity. Curve *c* is the AC impedance curve of the Au NPs@CoFe/N-GCT/CHIT/GCE incubated with the CRP antibody. The impedance increases further (R_{ct} = 700 Ω) due to the non-conductivity of the CRP antibody. Curve *d* is the AC impedance curve of anti-CRP/Au NPs@CoFe/N-GCT/CHIT/GCE with 1% BSA added dropwise to block non-specific sites. Since BSA is non-conductive, the impedance further increases (R_{ct} = 1150 Ω), curve *e* is the AC impedance curve of BSA/anti CRP/Au NPs@CoFe/N-GCT/CHIT/GCE incubated with the CRP antigen. Because the CRP antigen is not conductive, it hinders the transfer of electrons on the electrode surface, thus the impedance value increased greatly (R_{ct} = 1600 Ω). Curve *f* is the AC impedance curve of CRP/BSA/anti CRP/Au NPs@CoFe/N-GCT/CHIT/GCE after dropping the Au NPs/Cu(II)-HKUST-1/Tb labeled CRP antibody. The impedance value is the largest among the tested electrodes (R_{ct} = 2800 Ω), the electrochemical behaviors verify that the sensor layer-by-layer modification process is stable and successful.

Correspondingly, Fig. 6(B) is the cyclic voltammetric curves of different electrode modified interfaces measured in 5 mmol L^{-1} of $K_3Fe(CN)_6/K_4Fe(CN)_6$ solution. It can be found that the current value of bare GCE (curve *a*) is the largest and the current value of Au NPs@CoFe/N-GCT/CHIT/GCE (curve *b*) was because chitosan was used to modify the GCE. When the CRP antibody was cultivated on the electrode substrate, the current decreased, which is caused by the non-conductivity of protein anti-CRP (curve *c*). The current of BSA/anti-CRP/Au NPs@CoFe/N-GCT/CHIT/GCE (curve *d*) decreased further because BSA is a non-conductive substance. Similarly, when the target CRP antigen is added on the basis of the previous step, the current value of CRP/BSA/anti-CRP/Au NPs@CoFe/N-GCT/CHIT/GCE (curve *e*) also decreased. The reason why the current value of anti-CRP/CRP/BSA/anti-CRP/Au NPs@CoFe/N-GCT/CHIT/GCE (curve *f*) is the smallest is that the labeled antibody is added on the basis of the above electrode cultivation, which further hinders the surface of the GCE charge transfer. The above results show that the current value of the sensor decreases with the increase of the number of modified layers, which proves that the sensor is successfully constructed. These characterization results are consistent with those of the electrochemical impedance behaviour, which further proves the reliability of the experimental results.

Optimization of experimental conditions

Effect of pH on the response current value of the immunosensor

Due to the response signals of the sensor being different in different pH environments, the influence of PBS buffer solution

on the current response signals of the sensor is investigated in this experiment, and the response performance of the sensor in the pH range of 6.0–9.0 is explored. The results are shown in Fig. 7(A). It shows that the current response of the sensor reached the largest value when the pH was 7.5. Therefore, pH 7.5 was selected as the optimal pH for the rest of the experiments.

The effect of the immobilized CRP antibody concentration on the response current value of the immunosensor

The CRP antibody concentration immobilized on the electrode surface affects the current response value of the sensor. Therefore, it is necessary to optimize the CRP antibody concentration. As shown in Fig. 7(B), the response current of the electrode increases with the increase of CRP antibody concentration. When the antibody concentration reached 40 μg mL^{-1}, the current value was the largest. Then, the current value decreased slightly with the increase of antibody concentration and reached a plateau later. Therefore, 40 μg mL^{-1} was selected as the optimal concentration of immobilized antibody in this experiment.

Influence of CRP antigen incubation time on the response current of the immunosensor

The incubation time of the CRP antigen also affects the sensor response current. Therefore, the cultivation of the CRP antigen was optimized in this experiment. As shown in Fig. 7(C), the immobilized CRP antibody concentration was 40 μg mL^{-1}, and the response current of the electrode gradually increases with the increase of antigen incubation time. When the incubation time was 60 min, the response current reached the largest value. So, 60 min was chosen as the optimal antigen incubation time in this experiment.

The effect of the incubation time of the labeled antibody on the response current of the immunosensor

Under the conditions of fixing the optimal CRP antibody concentration, the antigen concentration and antigen incubation time, the incubation time of the labeled antibody was changed to investigate its influence on the sensor response current. As shown in Fig. 7(D), the incubation time of the labeled antibody was selected in the range of 15–90 min. As the incubation time of the labeled antibody increases, the response current value of the immunosensor gradually increases. When

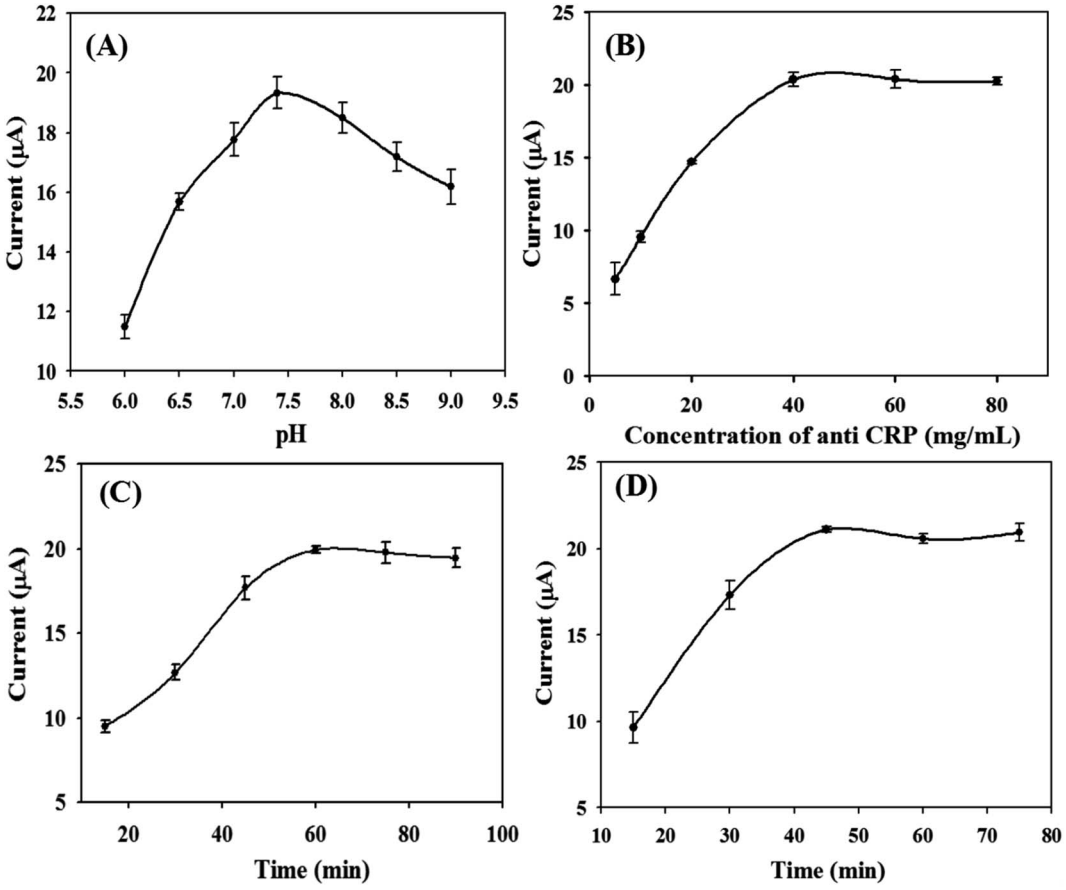

Fig. 7 Optimization of experimental conditions: (A) the effect of the pH of the buffer solution on the response current of the immunosensor; (B) the effect of the concentration of anti CRP immobilized on the electrode on the response current of immunosensor; (C) the effect of the incubation time of CRP on the response current of the immunosensor; and (D) the effects of incubation time of labeled anti-CRP on the response current of the immunosensor.

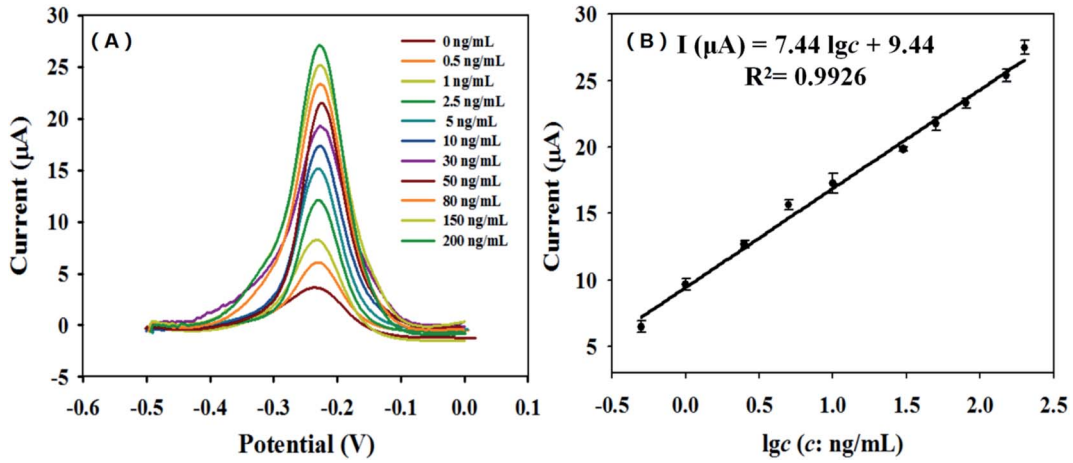

Fig. 8 The DPV response curves (A) and the calibration (B) of the CRP immunosensor (the concentrations of CRP were 0.5, 1, 2.5, 5, 10, 30, 50, 80, 150 and 200 ng mL^{-1}, respectively).

the incubation time reached 45 min, the response current value of the immunosensor reached the peak. After 45 min, the current value tends to be stable. Therefore, 45 min was chosen as the optimal incubation time for the labeled antibody.

Response performance of the CRP immunosensor

Under the optimal experimental conditions, the immunosensor was used to detect different concentrations of CRP antigens. Fig. 8(A) shows the DPV response curve of the immunosensor to different target concentrations. All data were measured in parallel 3 times, and the relative standard deviations are within 0.67–4.44%. As shown in Fig. 8(B), the response current value of the sensor is directly proportional to the concentration of the CRP antigen. The linear response range of the immunosensor is 0.5–200 ng mL^{-1}, the linear equation is $I(\mu A) = 7.44 \lg c + 9.44$, the linear correlation coefficient is 0.9926, and the detection limit is 166.7 pg mL^{-1}. Table 1 has displayed a comparison of proposed method with other methods for the detection of CRP. It can be seen from the Table 1 that the sandwich immunosensor developed in this experiment has good detection limit.

Selectivity of the CRP immunosensor

The selectivity and anti-interference ability of the sensor are important factors that reflect the performance of the sensor, the current response of the immunosensor to 200 ng mL^{-1} carcinoembryonic antigen (CEA), 200 ng mL^{-1} prostate specific antigen (PSA), 200 ng mL^{-1} human chorionic gonadotropin (HCG) and 200 ng mL^{-1} AFP antigen was tested in this experiment, and the result was compared with the response value to 20 ng mL^{-1} CRP antigen. The results are shown in Fig. 9(A). It can be seen from the figure that the response current value to 20 ng mL^{-1} CRP is the largest, while the response current values of the sensor to 200 ng mL^{-1} CEA, PSA, HCG and AFP antigen are all small, indicating that the CRP immunosensor has good selectivity.

The reproducibility, repeatability and stability of the CRP immunosensor

In order to investigate the reproducibility of the immunosensor, 10 electrodes were used to prepare the sensor separately and measure 20 ng mL^{-1} CRP antigen in this experiment. Each electrode was measured three times in parallel. The measurement results are shown in Fig. 9(B). The relative standard deviation (RSD) was 2.89% (n = 10), which shows that the immunosensor has good reproducibility. In order to investigate whether the sensor can be reused many times, the regeneration performance of the sensor was investigated in this experiment. The prepared electrode was used to detect 20 ng mL^{-1} of the

Table 1 A comparison of the proposed method with other methods for the detection of CRP

Method	Linear range	Detection limit	Reference
Surface plasmon resonance-based immunoassay	1.2–80 ng mL^{-1}	1.2 ng mL^{-1}	34
Label-free immunoassay	0.2–80 ng mL^{-1}	0.04 ng mL^{-1}	3
Micro-MEMS-fluxgate sensor	0.002–10 μg mL^{-1}	2 ng mL^{-1}	35
Aptamer-based colorimetry	0.889–20.7 μg mL^{-1}	1.2 μg mL^{-1}	11
Electrogenerated chemiluminescence (ECL)	—	1.2 μg mL^{-1}	36
Aptamer-based on microscope counting	0–70 nM	2.71 nM	37
Electrochemical immunosensor	0.5–200 ng mL^{-1}	0.167 ng mL^{-1}	This work

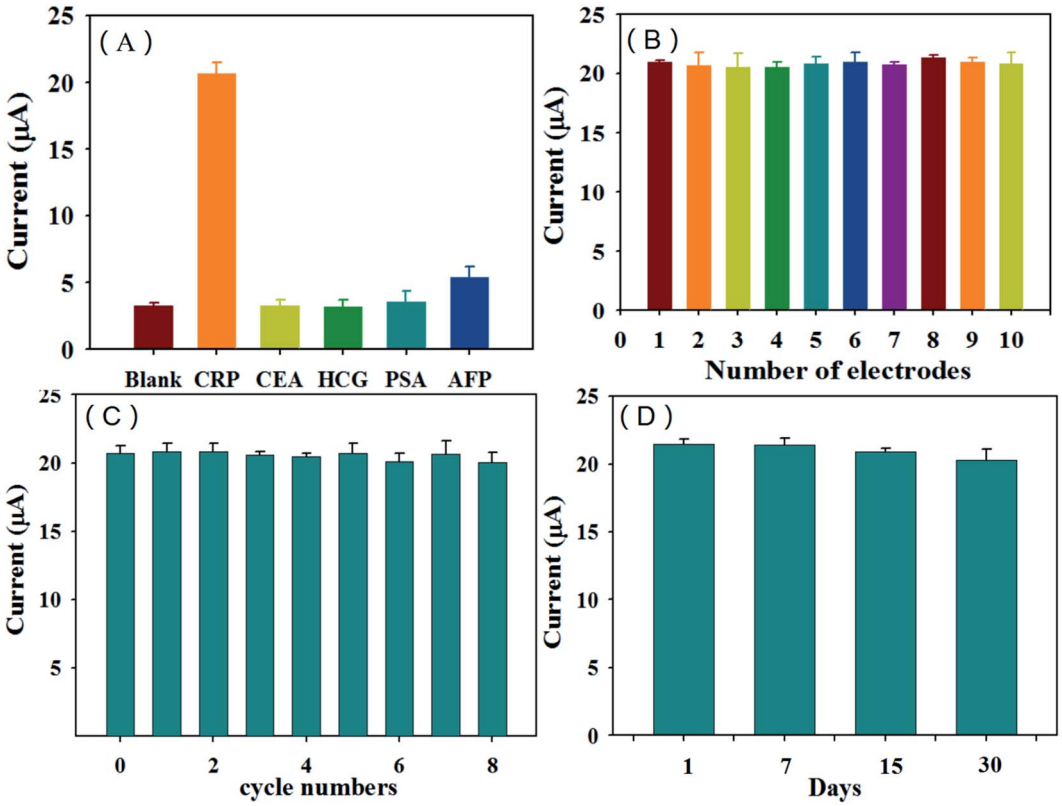

Fig. 9 The CRP immunosensor's selectivity (A), reproducibility (B), repeatability (C) and stability (D).

Table 2 Recovery of the CRP immunosensor

Sample	Added (ng mL^{-1})	Found (ng mL^{-1})	Recovery (%)	Average recovery (%)
1	5.00	4.90	98	99.77
2	50.00	51.35	102.7	
3	150.0	147.9	98.6	

CRP antigen. After the determination, the electrode was placed in 4 mol L^{-1} of urea solution for regeneration for 30 min. Then, it was washed with 0.5 mol L^{-1} of NaCl solution, dried after washing, and then the antigen and labeled antibody of the same concentration were re-incubated for determination. After the determination, the above operations were repeated. The results of this investigation are shown in Fig. 9(C). The immunosensor can be reused 8 times. After regenerating 8 times, the measured value is reduced to 96% of the original value (RSD = 1.46%, n = 3), which indicates that the immunosensor has good regeneration performance. To verify whether the sensor can be used for a long time, the stability of the sensor was investigated in this experiment. Three identical electrodes were prepared under the same conditions to determine 20 ng mL^{-1} of the CRP antigen. After the determination was complete, the electrode was eluted in 4 mol L^{-1} urea solution for 30 min, then rinsed with 0.5 mol L^{-1} NaCl solution, dried after rinsing, and finally stored in a refrigerator at 4 °C. After 7, 15 and 30 days, respectively, the electrode was re-incubated with the antigen and labeled antibody of the same concentration for the determination. The determination results are shown in Fig. 9(D). The determination value at 31 days is reduced to 94% of the original value (RSD = 2.72%, n = 3). The experimental results show that the immunosensor is stable and can be reused (Fig. 9).

Analysis of CRP in real serum

To investigate whether the immunosensor is suitable for CRP detection in real samples, three concentrations of CRP antigens were respectively selected and added to real dilute serum samples to determine the recovery rate. The results are shown in Table 2. The recovery rates of the three concentrations of CRP were in the range of 93.6–106.7%, and the relative standard deviations were within 5%, which indicates that the immunosensor is feasible for CRP detection in real samples.

Conclusions

In this paper, a novel sandwich immunosensor based on Au NPs/Cu(II)-HKUST-1/Tb and CoFe/N-GCT was constructed for the detection of CRP. An Au NPs@CoFe/N-GCT modified glassy carbon electrode was used as the substrate of the immunosensor to immobilize the CRP antibody on the electrode surface through Au–S bonds. The composite material (Au NPs/Cu(II)-HKUST-1/Tb) formed by the copper metal organic framework and Tb was used as the biomarker to label the antibody, thus

preparing a sandwich CRP immunosensor. This immunosensor has a low detection limit, good selectivity, wide detection range, good reproducibility and repeatability, and can be used repeatedly for a long time. This immunosensor can provide a fast, convenient and sensitive method for the quantitative determination of CRP.

Conflicts of interest

There are no conflicts to declare.

Acknowledgements

This work was supported by the National Natural Science Foundation of China (Grant No. 21465026, 21765026).

References

1 J. Park, S. Kurosawa, J. Watanabe and K. Ishihara, *Anal. Chem.*, 2004, **76**, 2649–2655.
2 S. K. Vashist, A. G. Venkatesh, E. M. Schneider, C. Beaudoin, P. B. Luppa and J. H. T. Luong, *Biotechnol. Adv.*, 2016, **34**, 272–290.
3 X. Zhang, R. Hu, K. L. Zhang, R. Y. Bai, D. L. Li and Y. H. Yang, *Anal. Methods*, 2016, **8**, 6202–6207.
4 Y. X. Zhang and O. J. Rojas, *Biomacromolecules*, 2017, **18**, 526–534.
5 K. Salminen, P. Gronroos, J. Eskola, E. Nieminen, H. Harm and S. Kulmala, *Electrochim. Acta*, 2018, **282**, 147–154.
6 L. Wang, *Med. Mal. Infect.*, 2020, **50**, 332–334.
7 Y. Ma, J. Yang, T. Yang, Y. Deng, M. Q. Gu, M. Wang, R. Hu and Y. H. Yang, *RSC Adv.*, 2020, **10**, 9723–9729.
8 W. L. Roberts, R. Sedrick, L. Moulton, A. Spencer and N. Rifai, *Clin. Chem.*, 2000, **46**, 461–468.
9 W. L. Roberts, L. Moulton, T. C. Law, G. Farrow, M. C. Anderson, J. Savory and N. Rifai, *Clin. Chem.*, 2001, **47**, 418–425.
10 R. J. Cui, H. C. Pan, J. J. Zhu and H. Y. Chen, *Anal. Chem.*, 2007, **79**, 8494–8501.
11 M. Antonio, R. Ferreira, R. Vitorino and A. L. Daniel-da-Silva, *Talanta*, 2020, **214**, 120868–120894.
12 S. K. Vashist, G. Czilwik, T. V. Oordt, F. V. Stetten, R. Zengerle, E. M. Schneider and J. H. T. Luong, *Anal. Biochem.*, 2014, **456**, 32–37.
13 J. Kim, J. Lee, S. Kim and W. Jung, *ACS Appl. Mater. Interfaces*, 2016, **8**, 29877–29882.
14 M. C. Diaz, H. Jiang, E. I. Kauppinen, R. Sharma and P. B. Balbuena, *J. Phys. Chem. C*, 2019, **123**, 30305–30317.
15 J. Noe, M. Nutz, J. Reschauer, N. Morell, I. Tsioutsios, A. Reserbat-Plantey, K. Watanabe, T. Taniguchi, A. Bachtold and A. Hoegele, *Nano Lett.*, 2018, **18**, 4136–4140.
16 W. Zhong, Q. Chen, F. Yang, W. Liu, G. Li, K. Xie and M. Ren, *J. Electroanal. Chem.*, 2019, **850**, 113392–113397.
17 M. C. Diaz, H. Jiang, E. Kauppinen, R. Sharma and P. B. Balbuena, *J. Phys. Chem. C*, 2019, **123**, 30305–30317.
18 A. Douglas, R. Carter, M. Li and C. L. Pint, *ACS Appl. Mater. Interfaces*, 2018, **10**, 19010–19018.
19 Y. Wang, H. Wang, J. Ye, L. Shi and X. Feng, *Chem. Eng. J.*, 2020, **383**, 1–12.
20 H. You, L. Bai, Y. Yuan, J. Zhou, Y. Bai and Z. Mu, *Biosens. Bioelectron.*, 2018, **117**, 706–712.
21 P. V. Araújo, K. I. Teixeira, L. D. Lanza, M. E. Cortes and L. T. A. Poletto, *Acta Odontol. Latinoam.*, 2009, **22**, 93–97.
22 C. Carbonell, I. Imaz and D. Maspoch, *J. Am. Chem. Soc.*, 2011, **133**, 2144–2147.
23 K. Srinivas, Y. Lu, Y. Chen, W. Zhang and D. Yang, *ACS Sustainable Chem. Eng.*, 2020, **8**, 3820–3831.
24 Y. Y. Xue, J. W. Zhang, Y. P. Li, H. P. Li, Y. Wang, S. N. Li, C. Jiang, M. C. Hu and Q. G. Zhai, *ACS Appl. Mater. Interfaces*, 2020, **12**, 4432–4442.
25 Z. Wan, D. Yang, J. Chen, J. Tian, T. T. Isimjan and X. Yang, *ACS Appl. Nano Mater.*, 2019, **2**, 6334–6342.
26 F. Zheng, D. Xiang, P. Li, Z. Zhang, C. Du, Z. Zhuang, X. Li and W. Chen, *ACS Sustainable Chem. Eng.*, 2019, **7**, 9743–9749.
27 L. H. M. Azmi, D. Williams and B. P. Ladewig, *Chem. Eng. Res. Des.*, 2020, **158**, 102–113.
28 S. Mosleh, M. R. Rahimi, M. Ghaedi and K. Dashtian, *Ultrason. Sonochem.*, 2016, **32**, 387–397.
29 J. Zhang, C. Su, X. Xie, P. Liuand and M. Enamul Huq, *RSC Adv.*, 2020, **10**, 37028–37034.
30 H. Zhao, M. Lei, T. Liu, T. H. Huang and M. Zhang, *Inorg. Chim. Acta*, 2020, **511**, 1–29.
31 X. Liu, L. Wang, P. Yu, C. Tian, F. Sun, J. Ma, W. Li and H. Fu, *Angew. Chem., Int. Ed.*, 2018, **57**, 16166–16170.
32 J. Kimling, M. Maier, B. Okenve, V. Kotaidis, H. Ballot and A. Plech, *J. Phys. Chem. B*, 2006, **110**, 15700–15707.
33 F. Xu, S. Xian, Q. Xia, Y. Li and Z. Li, *Adsorpt. Sci. Technol.*, 2013, **31**, 325–340.
34 S. K. Vashist, E. M. Schneiderc and J. H. T. Luong, *Analyst*, 2015, **140**, 4445–4452.
35 L. Guo, Z. Yang, S. Zhi, Z. Feng, C. Lei and Y. Zhou, *PLoS One*, 2018, **13**, 1–17.
36 K. Salminen, P. Gronroos, J. Eskola, E. Nieminen, H. Harm and S. Kulmala, *Electrochim. Acta*, 2018, **282**, 147–154.
37 Y. Zhao, J. Zhao, T. Jin, S. Sun, W. Liue and Y. Tan, *RSC Adv.*, 2019, **9**, 34293–34298.